Do Valine Side Chains Have an Influence on the Folding Behavior of β-Substituted β-Peptides?

by **Alice Glättli**[a]), **Dieter Seebach**[b]), and **Wilfred F. van Gunsteren***[a])

[a]) Laboratorium für Physikalische Chemie, Swiss Federal Institute of Technology, ETH Hönggerberg, HCI, CH-8093 Zürich (fax: +41 1 632 1039; e-mail: wfvgn@igc.phys.chem.ethz.ch)

[b]) Laboratorium für Organische Chemie, Swiss Federal Institute of Technology, ETH Hönggerberg, HCI, CH-8093 Zürich

The influence of valine side chains on the folding/unfolding equilibrium and, in particular, on the 3_{14}-helical propensity of β^3-peptides were investigated by means of molecular-dynamics (MD) simulation. To that end, the valine side chains in two different β^3-peptides were substituted by leucine side chains. The resulting four peptides, of which three have never been synthesized, were simulated for 150 to 200 ns at 298 and 340 K, starting from a fully extended conformation. The simulation trajectories obtained were compared with respect to structural preferences and folding behavior. All four peptides showed a similar folding behavior and were found to predominantly adopt 3_{14}-helical conformations, irrespective of the presence of valine side chains. No other well-defined conformation was observed at significant population in any of the simulations. Our results imply that β^3-peptides show a structural preference for 3_{14}-helices independent of the branching nature of the side chains, in contrast to what has been previously proposed on the basis of circular-dichroism (CD) measurements.

1. Introduction. – β-Peptides belong to a class of compounds sometimes alluded to as 'foldamers' [1][2], *i.e.*, non-natural products with a tendency to adopt specific, three-dimensional conformations. In recent years, β-peptides have attracted much attention because of their ability to form well-ordered secondary structures with as few as four β-amino acid residues [3–5], such as reverse turns and pleated sheets [6–10], and, most importantly, helical conformations with distinct H-bonding patterns such as the 3_{14}-helix [11–15], the *10/12*-helix [16–18], the *10*-helix [19], and the 2.5_{12}-helix [20][21]. Due to their remarkable resistance to proteolytic degradation both *in vitro* and *in vivo* [22–25] and the translocation ability across cell membranes of some of these compounds [26–28], β-peptides are also promising candidates for pharmaceutical applications as antibacterial or antimicrobial agents [29–33], inhibitors of fat and cholesterol absorption [34], or as antiproliferative and somatostatin-mimicking agents [35–38].

The ability to design β-peptides with a specific biological activity that depends on the formation of well-defined secondary and tertiary structures requires detailed insight into the relationship between the β-amino acid sequence and the three-dimensional structure of the peptide. The particular secondary structure of a β-peptide and its stability relative to other secondary-structural motifs depend, to a large part, on the type of amino acid side chains and the substitution pattern of the β-amino acids [16][39]. As β-amino acids contain an additional C-atom in the backbone, they offer a number of different substitution patterns involving the backbone C-atom (α or β) to

which the side chain is attached and the configuration(s) of the backbone stereogenic centers. *Ab initio* quantum-mechanical studies on blocked monomer units of β-peptides have suggested that the structural preferences of β-peptides can be derived from the conformational properties of the monomer and that different substitution patterns stabilize different helical conformations [40][41]. Similar quantum-mechanical studies on dimer, trimer, and pentamer models of β-peptides have suggested that the *10/12*-helix with alternating 10- and 12-membered H-bonded rings is intrinsically favored by unsubstituted β-peptides [42–44]. In these studies, it was also proposed that peptides with substitution exclusively a the β-C-atom (β^3-peptides) preferentially adopt a 3_{14}-helical conformation, while an alternating substitution pattern at the β- and α-C-atoms (β^2/β^3-peptides) stabilizes the *10/12*- over the 3_{14}-helix, which is in line with experimental observations based on NMR and circular dichroism (CD) spectroscopy [3][4][11][12][14–16][18][45] and with the results from molecular-dynamics (MD) folding studies of β-peptides [17][46][47]. The effect of substituents on the peptide conformation is twofold [16][39][44]: on one hand, substituents have an impact on the local conformational stability of the peptide (at residue level), on the other hand, they influence the conformational preference of the peptide by medium- to long-range electrostatic, *Van der Waals*, and steric inter-residue interactions. Substituents in an axial orientation relative to the helix axis are observed to destabilize the helix due to steric crowding with the peptide backbone, as predicted by the so-called 'fitting' theory [12][16]. Thus, the incorporation of geminally disubstituted residues in β-peptides leads to a breakdown of the helical conformation [12][48–50]. At the other hand, hydrophobic or salt-bridge interactions between side chains at positions $i/(i+3)$ stabilize the 3_{14}-helical conformation [14][51][52].

Recently, *Raguse et al.* [53] reported that branched side chains adjacent to the β-C-atom (*e.g.*, valine and isoleucine side chains) stabilize the 3_{14}-helical conformation of β^3-peptides. By replacing all leucine side chains in a β^3-decapeptide by valine side chains, a CD spectrum with the characteristic pattern for a 3_{14}-helix was observed, whereas the CD spectrum of the original peptide turned out to be quite different [53]. Based on these results, the authors concluded that β-peptides constructed exclusively from β^3-amino acids may adopt conformations other than 3_{14}-helices. Similar observations, *i.e.*, that the 3_{14}-helical propensity of a β-peptide is enhanced in the presence of valine side chains, have also been made previously by *Hamuro et al.* [29] and *Gung et al.* [54]. However, these conclusions were all drawn on the basis of CD spectra only, in the absence of high-resolution structural NMR data. In the case of – compared to proteins – small and highly flexible peptides, CD spectroscopic data can be misleading [15][48][50][55–57].

In the present study, the effect of valine side chains on the structural preference of β^3-peptides is investigated by means of MD simulation, which not only provides an atomic-resolution picture, but also gives insight into dynamic processes such as those maintaining the folding/unfolding equilibrium of a peptide. Unbiased MD simulations have previously proven to correctly reproduce the experimentally determined structures of several β-peptides and to complement experimental findings [10][13][17][46][47][50][58]. Due to the relatively small size of these peptides, it is also feasible to study the folding/unfolding equilibrium by atomistic simulation and to characterize not only the folded, but also the unfolded states of peptides [46][58–60].

Here, the folding/unfolding equilibrium of two different β^3-heptapeptides containing valine side chains (peptides A_{val} and B_{val}; *Fig. 1*) is studied and compared to the folding behavior of their respective derivatives where the valine side chains were replaced by leucine side chains (peptides A_{leu} and B_{leu}) with the aim of addressing the following questions. Does the presence of side chains with branching adjacent to the β-C-atom (*i.e.*, valine side chains) influence the folding behavior of β^3-peptides and the stability of the 3_{14}-helical conformation? And if so, how do they influence the 3_{14}-helical propensity of β^3-peptides? Do β^3-peptides without valine side chains show structural preferences other than for the 3_{14}-helix?

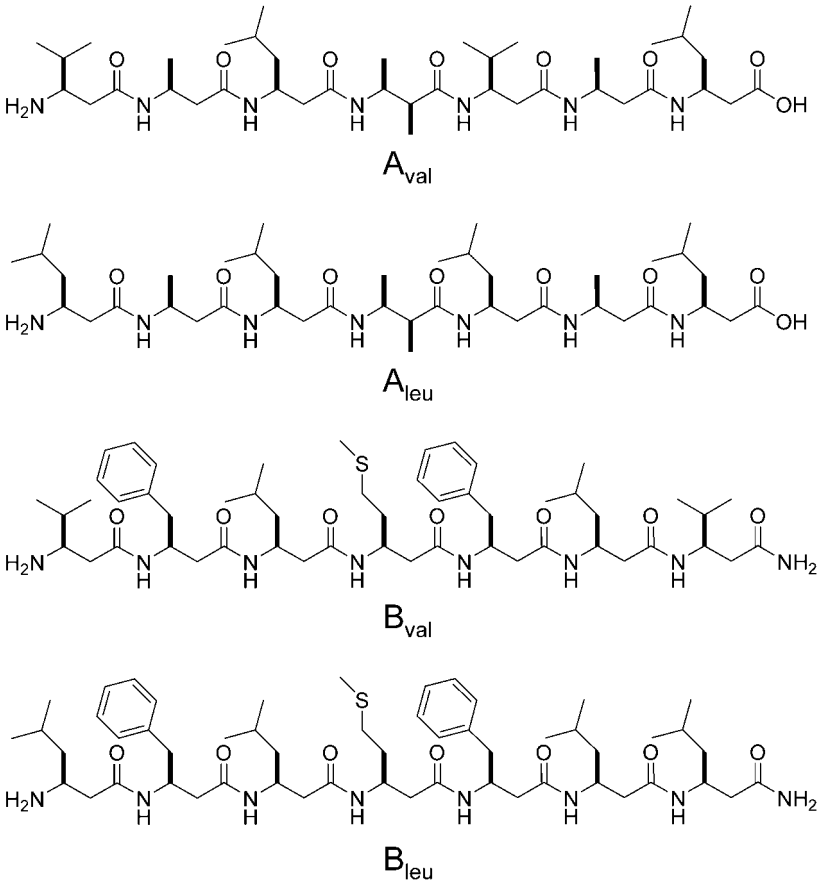

Fig. 1. *Chemical formulae of the β-heptapeptides studied*. Sequences: peptide A_{val}: NH_2-β-HVal–β-HAla–β-HLeu–β-HAla(αMe)–β-HVal–β-HAla–β-HLeu-OH; Peptide A_{leu}: NH_2-β-HLeu–β-HAla–β-HLeu–β-HAla(αMe)–β-HLeu–β-HAla–β-HLeu-OH; Peptide B_{val}: NH_2-β-HVal–β-HPhe–β-HLeu–β-HMet–β-HPhe–β-HLeu–β-HVal-NH_2; Peptide B_{leu}: NH_2-β-HLeu–β-HPhe–β-HLeu–β-HMet–β-HPhe–β-HLeu–β-HLeu-NH_2. Note that, in the simulations, both the N- and the carboxylic acid C-termini are protonated, in line with experimental data

Of the four peptides chosen for this study, peptide A_{val} had been previously investigated under various points of view [13][46][58][61–63]. A_{val} is well-charac-

terized both experimentally [11][12][16] and by MD simulation [13][46], and adopts a very stable 3_{14}-helical conformation in MeOH solution. No experimental data were available for peptides A_{leu}, B_{val}, and B_{leu}. The two sets A_{val}/A_{leu} and B_{val}/B_{leu} differ from the set studied by *Raguse et al.* [53]. However, if the effect of valine and similar side chains is generally valid for β^3-peptides, substituting the valine side chains in the peptides A_{val} and B_{val} by leucine side chains is expected to affect their folding behavior, too. The formation of a 3_{14}-helix by peptide B_{val} can be expected from the large number of experimental and theoretical studies showing that an all-β^3-peptide predominantly adopts a 3_{14}-helical conformation in solution.

All four peptides were simulated at a pressure of 1 atm and at temperatures of 298 and 340 K, using the GROMOS force field [64][65] (version 45A3) and the GROMOS simulation software [64][66]. The simulation at elevated temperature allows the sampling of more unfolding/folding events and, thus, gives statistically more-relevant results. The initial conformation was chosen to be fully extended for all four peptides. The resulting *Boltzmann*-weighted ensembles of structures were analyzed in terms of structural properties such as H-bonding and torsional-angle distributions, folding/unfolding behavior, and with respect to the stability of the 3_{14}-helical conformation (see *Exper. Part*).

2. Results and Discussion. – 2.1. *Hydrogen Bonds and Conformational Analysis.* A total of eight 150- to 200-ns-long MD simulations (*Table 1*) on the four β-heptapeptides shown in *Fig. 1* were performed with the aim of studying the effect of the presence of valine side chains on the folding behavior of β-peptides. As the secondary structures of β-peptides, in particular the various helices, are strongly related to their H-bond patterns, a H-bond analysis was performed on the resulting simulation trajectories. The corresponding results are presented in *Table 2*, where the intramolecular H-bond populations are listed. The analysis shows that, in all four peptides, at both 298 and 340 K, the predominant H-bonds are of the type $i/(i+2)$, *i.e.* H-bonds are formed between the NH group of residues i and the carbonyl O-atoms of residues $(i+2)$, resulting in 14-membered H-bonded rings (denoted as HB_{14}), characteristic for 3_{14}-helical conformations. In addition, some 18- and 22-membered H-bonded rings (HB_{18} and HB_{22}) are observed, along with H-bonds between the NH group of residue 6 and the carbonyl O-atom of residue 3, which would correspond to a central H-bond in a right-handed 2.5_{12}-helix. However, the latter three H-bond types are all rather weakly populated. Comparison of the HB_{14}-type H-bond populations of peptide A_{val} with those of peptide A_{leu} shows that, in the simulations at 298 K (simulations $A_{val\text{-}298}$ and $A_{leu\text{-}298}$), the central H-bonds NH(2)$\cdots$O(4), NH(3)$\cdots$O(5), and NH(4)$\cdots$O(6) are about twice as strongly populated in the ensemble of structures of peptide A_{val} as in that of A_{leu}. At 340 K, however, the central H-bonds are only 10% more populated in peptide A_{val}. For the peptides B_{val} and B_{leu}, the differences in HB_{14} H-bond populations are similar at both temperatures. The H-bonds NH(2)$\cdots$O(4) and NH(3)$\cdots$O(5) are between 17 and 22% less populated in peptide B_{leu} than in B_{val}, whereas the H-bond between residues 4 and 6 in peptide B_{leu} at room temperature is 3% more and, at elevated temperature, 11% less populated, respectively, than in peptide B_{val}. In summary, the dominant H-bonds observed in all eight ensembles of structures are characteristic of 3_{14}-helical conformations, irrespective of the presence of valine side

Table 1. *Overview of the MD Simulations Performed*

Peptide	Simulation	Number of solvent molecules	Temperature [K]	Simulation time [ns]
A_{val}	$A_{val\text{-}298}$	1778	298	200
	$A_{val\text{-}340}$	1778	340	200
A_{leu}	$A_{leu\text{-}298}$	1845	298	200
	$A_{leu\text{-}340}$	1845	340	150
B_{val}	$B_{val\text{-}298}$	1862	298	200
	$B_{val\text{-}340}$	1862	340	200
B_{leu}	$B_{leu\text{-}298}$	1864	298	200
	$B_{leu\text{-}340}$	1864	340	150

Table 2. *Intramolecular H-Bond Populations* (in %). Only H-bonds with a population larger than 5% in at least one of the eight simulations are reported. A H-bond is considered to exist when the donor – H-atom – acceptor angle is larger than 135° and the H-atom – acceptor distance is smaller than 0.25 nm. The H-bonds are grouped according to the size of the resulting H-bonded ring (*e.g.*, a H-bond between NH(i) and C=O($i+2$) results in a 14-membered H-bonded ring denoted as HB_{14}).

Donor ··· Acceptor	$A_{val\text{-}298}$	$A_{val\text{-}340}$	$A_{leu\text{-}298}$	$A_{leu\text{-}340}$	$B_{val\text{-}298}$	$B_{val\text{-}340}$	$B_{leu\text{-}298}$	$B_{leu\text{-}340}$
NH(i) ··· O($i+2$) [HB_{14}]								
NH(1) ··· O(3)	19	18	17	18	16	17	18	18
NH(2) ··· O(4)	49	44	21	39	55	42	45	34
NH(3) ··· O(5)	56	50	22	42	58	46	48	36
NH(4) ··· O(6)	54	42	26	39	64	52	66	46
NH(5) ··· O(7)	17	11	11	13	57	46	58	42
NH(i) ··· O($i+3$) [HB_{18}]								
NH(1) ··· O(4)	6	5	13	6	5	6	8	10
NH(3) ··· O(6)	4	5	8	4	1	1	1	2
NH(i) ··· O($i+4$) [HB_{22}]								
NH(1) ··· O(5)	4	4	13	6	3	3	5	8
NH(2) ··· O(6)	3	3	11	4	2	1	1	5
NH(3) ··· O(7)	2	1	6	2	1	2	4	6
NH(i) ··· O($i-3$) [HB_{12}]								
NH(6) ··· O(3)	0	0	2	1	2	7	2	1

chains. This is a strong indication that all four peptides fold to a 3_{14}-helix in MeOH solution. Still, it is evident that the central HB_{14}-type H-bonds tend to be present more frequently in the ensembles of structures of the peptides with valine side chains. However, it should also be noted that the differences in H-bond populations are more pronounced at 298 K than at 340 K.

The atom-positional root-mean-square deviation (rmsd) of the backbone atoms (N, C_β, C_α, C) of residues 2 to 6 from a 3_{14}-helical model structure is shown in *Fig. 2* for all eight simulation trajectories as a function of simulation time. All peptides are observed to fold to a 3_{14}-helix, and then to repeatedly unfold and refold to 3_{14}-helical conformations. From the rmsd plots, it is also obvious that, in all simulations, except for $A_{leu\text{-}298}$, the 3_{14}-helix corresponds to the most-populated conformer. As expected, the initial folding process is slower at room temperature than at elevated temperature. At 298 K, the folding to the 3_{14}-helix takes place between 15 and 80 ns, while, at 340 K, the peptides all fold within the first 15 ns. The initial folding time to reach the 3_{14}-helix

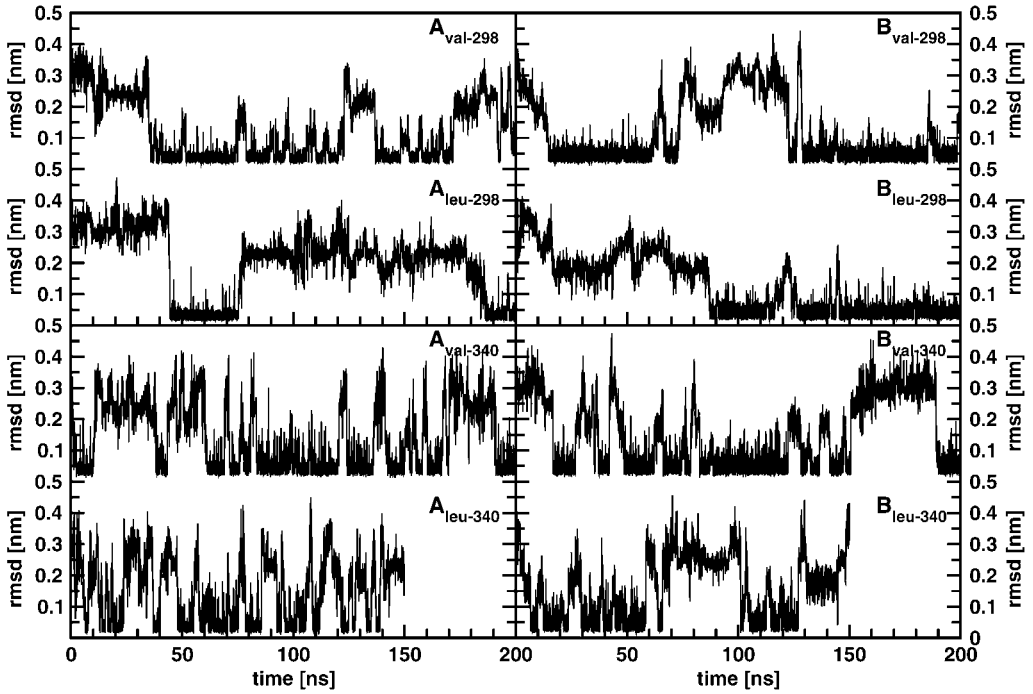

Fig. 2. *Root-mean-square difference* (rmsd) *of the peptide backbone atoms of residues 2 to 6 as a function of time and temperature with respect to the* 3_{14}*-helical conformation*. For peptide A_{val}, the NMR model structure was used as the 3_{14}-helical reference structure; for all other peptides, a canonical 3_{14}-helical conformation was taken as reference

at room temperature appears to be longer for A_{leu} and B_{leu}, containing no valine side chains. A_{leu} folds after 45 ns at 298 K, while A_{val} is observed to fold after *ca*. 32 ns. The difference in initial folding time is more pronounced for peptides B_{val} and B_{leu}: B_{val} folds to the 3_{14}-helix within the first 15 ns, while, in the absence of valine side chains (peptide B_{leu}), the peptide requires 82 ns of simulation time to fold. However, these differences in initial folding times should not be considered as resulting from the presence of valine side chains, since they are statistically irrelevant when only one event is considered. In addition, the initial folding times of the peptides A_{leu} and B_{leu} at elevated temperature are comparable to the initial folding times of the peptides with valine side chains.

To determine which conformers the peptides adopt during the simulation, a conformational-clustering analysis was performed over each simulation trajectory. Such an analysis groups the structures of an ensemble according to their atom-positional rmsd of the backbone atoms of residues 2 to 6 between each pair of structures. A similarity criterion of 0.1 nm was employed. To avoid spreading of the 3_{14}-helical conformations over more than one cluster, the NMR model structure, when available, or a canocnial 3_{14}-helix was imposed during the clustering process as central-member structure of a cluster. In *Figs. 3* and *4*, the central-member structures of the three most-populated clusters (conformers) are shown together with their population.

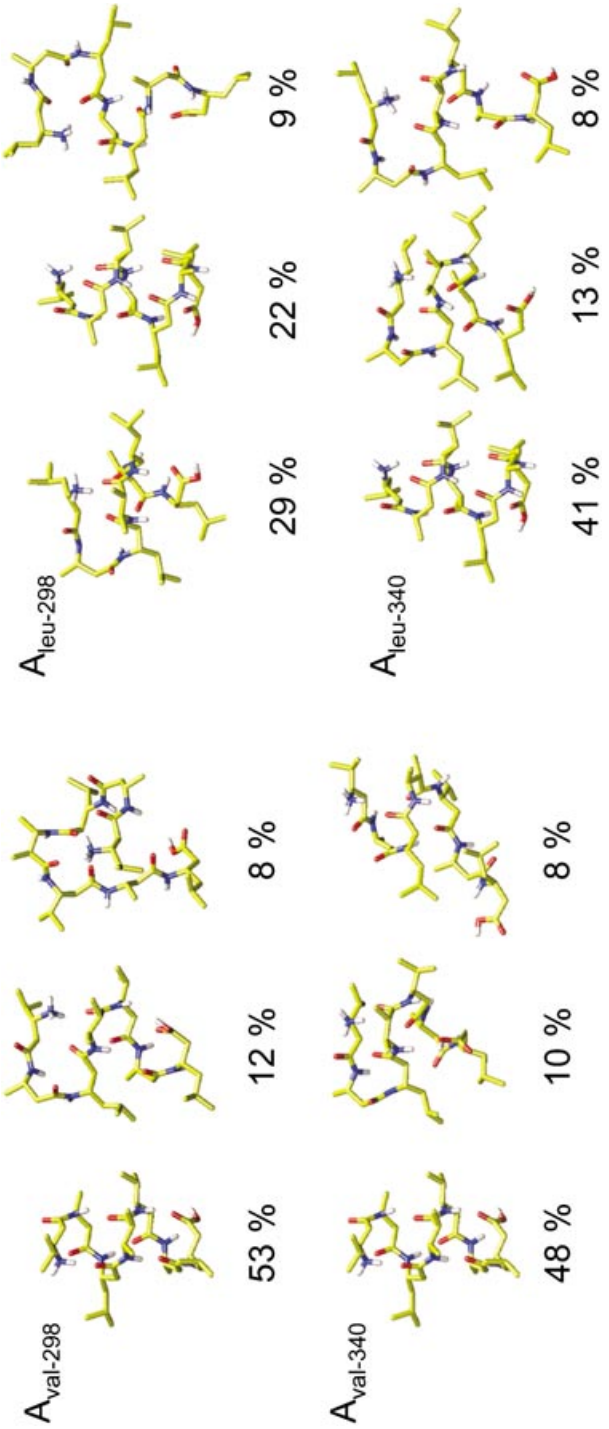

Fig. 3. *Conformational preferences of peptides A_{val} and A_{leu}.* The three most-populated conformers (central structures of the three most-populated clusters with a backbone (residues 2 to 6) rmsd similarity criterion of 0.1 nm) observed in the simulations at 298 and 340 K are shown. For each conformer, its corresponding population is indicated. Atom coloring: C, yellow; H, white; N, blue; O, red.

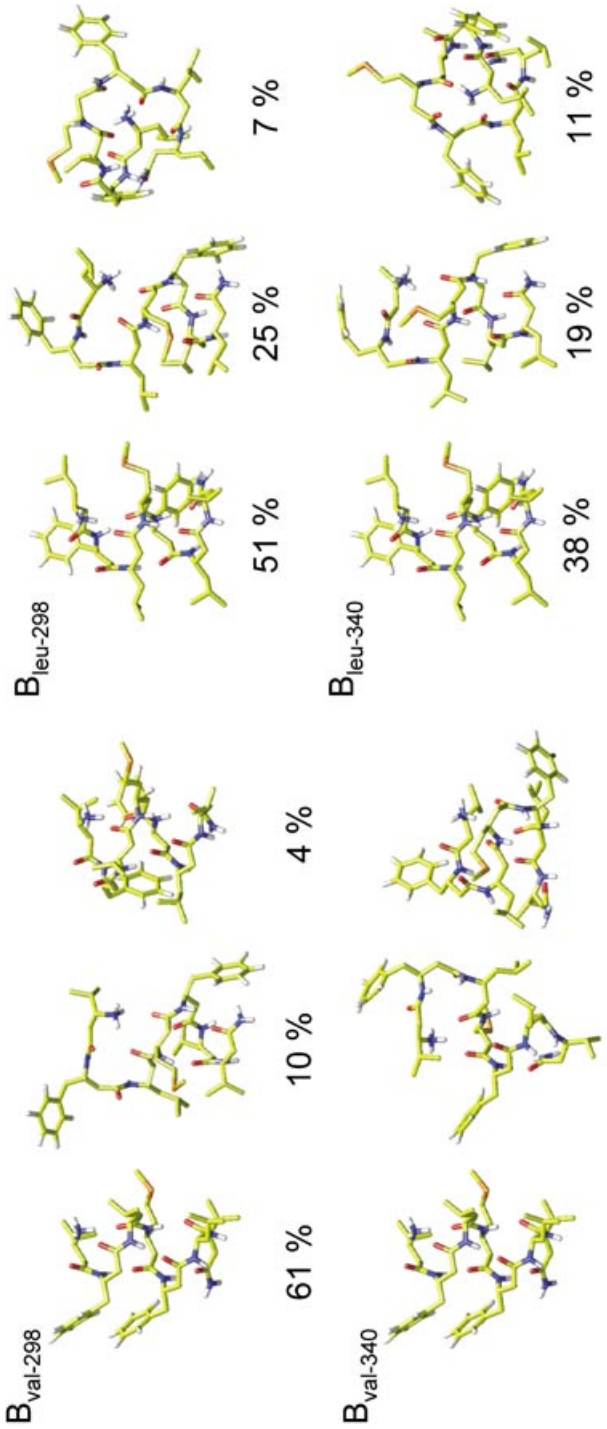

Fig. 4. *Conformational preferences of peptides B_{val} and B_{leu}.* The three most-populated conformers (central structures of the three most-populated clusters with a backbone (residues 2 to 6) rmsd similarity criterion of 0.1 nm) observed in the simulations at 298 and 340 K are shown. For each conformer, its corresponding population is indicated. Atom coloring: C, yellow; H, white; N, blue; O, red; S, orange.

The cluster representing the 3_{14}-helix corresponds to the most-populated conformer in all but one of the simulations: in $A_{leu\text{-}298}$, the most-populated conformer corresponds to structures with some 18- and 22-membered H-bonded rings (NH(3)···O(6), NH(1)···O(5), and NH(2)···O(6)), while the second-most-populated cluster represents the 3_{14}-helical conformations (*Fig. 3*). In simulation $A_{val\text{-}298}$, the second-most-populated cluster corresponds to a 3_{14}-helical conformation dominated by the H-bonds NH(4)···O(6) and NH(5)···O(7), with a nonfolded N-terminus. Similar conformers are observed in the simulations $A_{leu\text{-}298}$ and $A_{leu\text{-}340}$, representing the third-most-populated cluster. In simulation $A_{val\text{-}340}$, the third-most-populated conformer also corresponds to a partially unfolded 3_{14}-helix, with the central H-bonds NH(2)···O(4) and NH(3)···O(5) retained. The main conformers besides the 3_{14}-helix of peptides B_{val} and B_{leu} have similar structures (*Fig. 4*). They correspond either to some 'collapsed' structure containing 18- and 22-membered H-bonded rings (cluster 3 in simulations $B_{val\text{-}340}$, $B_{leu\text{-}298}$, and $B_{leu\text{-}340}$), or they represent a partly folded 3_{14}-helix with the characteristic C-terminal H-bonds retained. Based on CD-spectroscopic measurements, *Raguse et al.* [53] suggested that β^3-peptides without valine side chains or, more generally, without α-branched side chains adjacent to the β-C-atom, may adopt well-defined structures other than the 3_{14}-helix. In the simulations presented here, we indeed also observe 2.5_{12}-helical turns, but at a very low statistical weight ($< 3\%$) and, remarkably, for both peptides B_{val} and B_{leu}. In summary, we note that the main conformers adopted by the four peptides in the course of the simulations are very similar, and no significantly populated, well-defined structure other than the 3_{14}-helix is observed.

2.2. *Thermodynamic and Kinetic Properties of the 3_{14}-Helical Conformations.* On the basis of the conformational-clustering results, the ranking, the percentage weight of the 3_{14}-helical conformation in the ensemble, and the estimated free energy of folding to the 3_{14}-helix, along with the kinetic properties of this folding process, were evaluated in all eight simulations (*Table 3*). The kinetic properties such as the average lifetime of the 3_{14}-helix, the number of (re)folding events, the average (re)folding time to the 3_{14}-helical conformation, and the average number of conformers visited during the (re)folding process were calculated from the time sequence of sampling of conformers (clusters), as described in the *Exper. Part*. Since, in the simulation $A_{leu\text{-}298}$, the 3_{14}-helix does not correspond to the most-populated conformer, the thermodynamic and kinetic properties evaluated for the 3_{14}-helix are also calculated for the most-populated conformer (referred to as MPC in *Table 3*). At room temperature, the 3_{14}-helix is much less populated for peptide A_{leu} than for peptide A_{val} (22 *vs.* 53%), which is in line with the 3_{14}-helix-characteristic H-bond populations observed. In addition, simulation $A_{leu\text{-}298}$ shows a longer average lifetime of the 3_{14}-helix and an average folding time to the helix is up to four times longer. Thus, fewer folding events are observed during the simulation $A_{leu\text{-}298}$ as compared to the other three simulations. Considering that the folding behavior of the two peptides A_{val} and A_{leu}, as well as the populations of the 3_{14}-helix, are comparable at 340 K, the difference in population and in folding kinetics at room temperature may be rather due to the poor statistics at room temperature than due to the effect of the valine side chains. For peptides B_{leu} and B_{val}, the folding behavior and thermodynamic stability of the 3_{14}-helix are comparable at both simulation temperatures. Compared to peptide B_{val}, the 3_{14}-helical conformation is 10–12% less populated in both simulations of peptide B_{leu}, which is in the order of the

Table 3. *Folding Behavior of the Four Peptides Studied*. For every simulation (see *Table 1*), the number of conformers and the (re)folding properties of the 3_{14}-helical conformation and of the most-populated conformer (MPC) are listed as obtained from the conformational-clustering analysis [58]. In all simulations, except for $A_{leu\text{-}298}$, the 3_{14}-helix corresponds to the most-populated conformer, $N_{conf}^{100\%}$, total number of conformers; $N_{conf}^{99\%}$, $N_{conf}^{95\%}$, $N_{conf}^{75\%}$, and $N_{conf}^{50\%}$, total numbers of conformers with a combined weight of 99, 95, 75, and 50%, resp.; $\Delta G_{fold}^{3_{14}\text{-helix}}$ and ΔG_{fold}^{MPC}, estimated free energy of folding to the 3_{14}-helix and the MPC, resp.; $\langle \tau^{3_{14}\text{-helix}} \rangle$ and $\langle \tau^{MPC} \rangle$, average lifetimes; $\langle t_{fold}^{3_{14}\text{-helix}} \rangle$ and $\langle t_{fold}^{MPC} \rangle$, average times of (re)folding to the 3_{14}-helix and to the MPC, resp.; $\langle Con_{visited} \rangle$, average number of conformers visited during (re)folding. Note that the helical cluster is denoted by cluster sequence number 0, but may have the ranking 1 if it corresponds to the MPC.

	$A_{val\text{-}298}$	$A_{val\text{-}340}$	$A_{leu\text{-}298}$	$A_{leu\text{-}340}$	$B_{val\text{-}298}$	$B_{val\text{-}340}$	$B_{leu\text{-}298}$	$B_{leu\text{-}340}$
$N_{conf}^{100\%}$	145	319	276	298	163	378	83	287
$N_{conf}^{99\%}$	68	179	159	170	80	229	35	174
$N_{conf}^{95\%}$	25	77	75	73	36	101	13	76
$N_{conf}^{75\%}$	4	7	12	8	4	7	2	5
$N_{conf}^{50\%}$	1	2	2	2	1	1	1	2
Ranking of 3_{14}-helix	1	1	2	1	1	1	1	1
Weight of 3_{14}-helix [%]	53	48	22	41	61	50	51	38
$\Delta G_{fold}^{3_{14}\text{-helix}}$ [kJ mol^{-1}]	−0.3	0.2	3.1	1.0	−1.1	0.0	−0.1	1.4
$\langle \tau^{3_{14}\text{-helix}} \rangle$ [ps]	959	825	1829	624	2476	1310	1935	863
No. of folding events to 3_{14}-helix	112	117	23	100	49	76	45	67
$\langle t_{fold}^{3_{14}\text{-helix}} \rangle$ [ps]	1763	1693	6986	1205	2324	1454	2239	1432
$\langle Con_{visited} \rangle$ during folding to 3_{14}-helix	7	19	18	14	9	12	5	11
Weight of MPC [%]	53	48	29	41	61	50	51	38
ΔG_{fold}^{MPC} [kJ mol^{-1}]	−0.3	0.2	2.2	1.0	−1.1	0.0	−0.1	1.4
$\langle \tau^{MPC} \rangle$ [ps]	959	825	484	624	2476	1310	1935	863
No. of folding events to MPC	112	117	124	100	49	76	45	67
$\langle t_{fold}^{MPC} \rangle$ [ps]	1763	1693	938	1205	2324	1454	2239	1432
$\langle Con_{visited} \rangle$ during folding to MPC	7	19	5	14	9	12	5	11

fluctuations of the conformer population (see below). In all simulations, the kinetically most-stable conformer corresponds to the 3_{14}-helix, even in simulation $A_{leu\text{-}298}$ where a conformer other than the 3_{14}-helix represents the most-populated and, thus, thermodynamically most-stable conformer.

Certainly, the properties presented in *Table 3* are only meaningful if the simulations have converged. To assess this, the number of conformers (clusters) with a 99, 95, 75, and 50% joined weight in the ensemble is plotted as a function of time in *Fig. 5*. The reason to plot the number of clusters with 99% weight rather than with 100% weight is to exclude most of the singly populated clusters from the conformation count. Singly populated clusters are generally not isolated in the rmsd space, but lie at the border of other clusters. This is a consequence of the clustering criterion that no member of a cluster may differ by more than a given rmsd threshold value from the central member of the cluster. Therefore, singly populated clusters should be considered as an artifact of the clustering algorithm. Although the number of clusters with a 99% weight seems to have largely converged for most of the simulations, a sudden increase in this number with more simulation time, as observed for simulation $B_{val\text{-}340}$, cannot be excluded. However, it is unlikely that the number of clusters will evolve to more than 500 conformers when extending the simulations. On the other hand, the number of conformers with 75 and 50% weight seem to have converged.

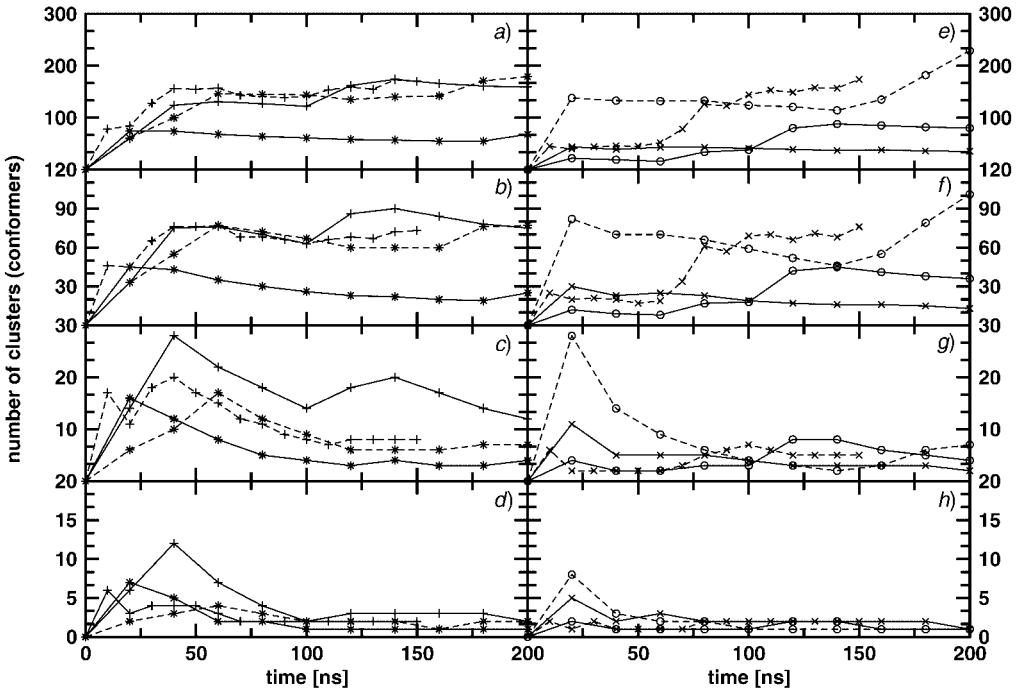

Fig. 5. *Number of clusters as a function of time.* Panels *a*)–*d*): number of clusters in the simulations $A_{val\text{-}298}$ (∗ — ∗), $A_{val\text{-}340}$ (∗---∗), $A_{leu\text{-}298}$ (+ — +) and, $A_{leu\text{-}340}$, (+---+) with a combined weight of 99% (*a*), 95% (*b*), 75% (*c*), and 50% (*d*), respectively. Panels e)–h): number of clusters in the simulations $B_{val\text{-}298}$ (○—○), $B_{val\text{-}340}$ (○---○), $B_{leu\text{-}298}$ (× — ×), and $B_{leu\text{-}340}$ (× --- ×) with a combined weight of 99% (*e*), 95% (*f*), 75% (*g*), and 50% (*h*), resp.

In *Fig. 6*, the percentage weight of the 3_{14}-helical conformation in the ensemble is shown as a function of time for the different simulations in order to assess the convergence of the sampling of the 3_{14}-helix. Two statements can be made on this basis: first, even after 200 ns of simulation, it may be difficult, particularly for the simulations at 298 K, to assess whether the relative population of the 3_{14}-helix has converged. Compared to the simulation at 340 K, a larger population of the 3_{14}-helical conformation is expected at room temperature. Thus, simulation $A_{leu\text{-}298}$ has probably not converged yet. Second, considering the last 75 ns of the simulations, the average fluctuation of the helix population is estimated to lie between 5 and 15% for the different simulations. This should be taken into account when comparing the populations of the peptide with and without valine side chains.

2.3. *The Influence of Valine Side Chains on the Accessible Structural and Dihedral-Angle Conformational Space.* All peptides studied here predominantly adopt a 3_{14}-helical conformation in the simulations, irrespective of the presence of valine side chains. The helix represents the conformer with the longest average lifetime. In many cases, the three most-populated clusters observed in the simulations are structurally rather similar to each other. Nevertheless, it is worthwhile to investigate how much the conformational spaces sampled by the simulations of the peptides A_{val} and A_{leu} overlap

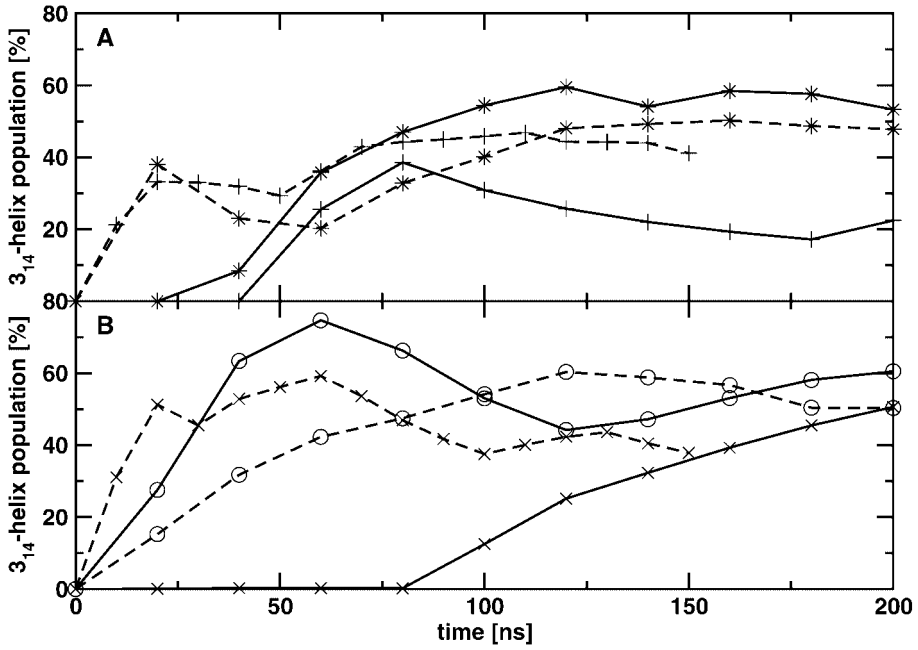

Fig. 6. *Population of the* 3_{14}*-helical conformation as a function of time. a*) Simulations $A_{val\text{-}298}$ (*—*), $A_{val\text{-}340}$ (*---*), $A_{leu\text{-}298}$ (+—+), and $A_{leu\text{-}340}$ (+---+); *b*) simulations $B_{val\text{-}298}$ (o—o), $B_{val\text{-}340}$ (o---o), $B_{leu\text{-}298}$ (×—×), and $B_{leu\text{-}340}$, (×---×).

(and similarily B_{val} and B_{leu}). To this end, a conformational clustering analysis over the concatenated trajectories from the simulations $A_{val\text{-}298}$ and $A_{leu\text{-}298}$ (40000 structures), $A_{val\text{-}340}$ and $A_{leu\text{-}340}$ (35000 structures), $B_{val\text{-}298}$ and $B_{leu\text{-}298}$ (40000 structures), and $B_{val\text{-}340}$ and $B_{leu\text{-}340}$ (35000 structures) has been performed by means of the same rmsd similarity criterion as for the analysis over the individual trajectories, and the compositions of the resulting clusters were analyzed. The corresponding results are presented in *Fig. 7*, where the populations of the resulting clusters are displayed together with the fraction that belongs to the single MD trajectories. Note that, for the clustering analysis over the combined trajectories at 340 K, 20000 structures originate from the simulations of the peptides with valine, and 15000 structures from those with leucine side chains, respectively. The by far most-populated cluster in all four combined ensembles represents the 3_{14}-helix. The clusters with large populations in all four ensembles contain structures from both peptides, indicating that the conformational spaces of A_{val} and A_{leu}, and of B_{val} and B_{leu}, respectively, overlap to a large part. Only a few clusters of rather low weight are observed to exclusively contain structures from one or the other ensemble. However, all of them represent essentially non-ordered conformers.

Recently, *Martinek* and *Fülöp* [39] tried to rationalize the presumably larger 3_{14}-helical propensity of β^3-peptides with valine side chains. Based on molecular-mechanical calculations, they evaluated the torsional potential energy of the $C(O)-N-C_\beta-C_\alpha$ torsional angle for different β^3-substituents (Val, Ala, Leu). With valine side chains, the energy minimum at a torsional angle ϕ of 60° as well as the

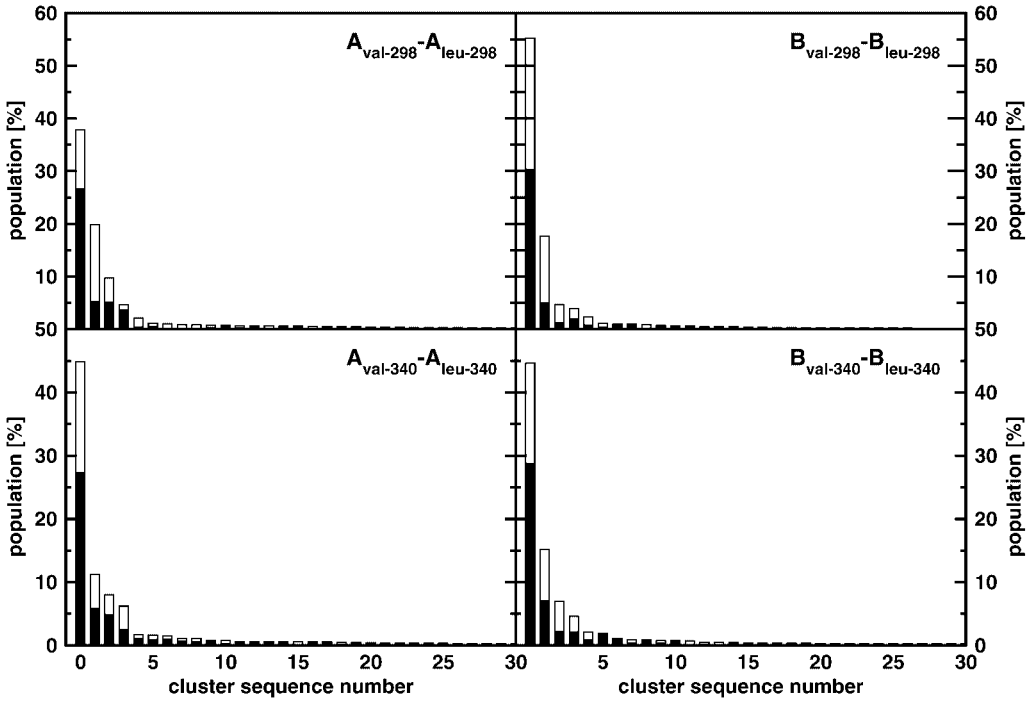

Fig. 7. *Conformational analysis over the combined trajectories of the peptides A_{val} and A_{leu} at 298 and 340 K* ($A_{val\text{-}298} - A_{leu\text{-}298}$ and $A_{val\text{-}340} - A_{leu\text{-}340}$), *and of B_{val} and B_{leu} at 298 and 340 K* ($B_{val\text{-}298} - B_{leu\text{-}298}$ and $B_{val\text{-}340} - B_{leu\text{-}340}$). The plot shows the population in percentage per conformer (cluster) and the portion of structures per cluster that belong to the trajectories of the peptides with either valine side chains (black) or leucine side chains (white). Cluster 0 represents the 3_{14}-helical conformation.

barrier between 60° and −120° were increased, making the dihedral-angle conformation near 60° inaccessible for the backbone. Thus, the authors argued that, as the steric demand of the β^3-substituent in the proximity of the adjacent amide group increases, the accessible conformational space decreases for the above torsion. To test whether the β^3-peptides without valine side chains, indeed, access a larger torsional space than those with valine side chains, the distribution of the three backbone (ϕ, θ, Ψ) and first side-chain (χ) dihedral angles for residues 1–7 are displayed in *Fig. 8* for the peptides A_{val} and A_{leu}, and in *Fig. 9* for B_{val} and B_{leu}. The distributions of the backbone dihedral angles appear to be rather similar and seem to be independent of the nature of the β^3-substituent. All torsions $C(O)-N-C_\beta-C_\alpha$ (ϕ) are centered around −120°, and there are only very small, if any at all, populations around 60°. Only in simulation $A_{leu\text{-}298}$, a population of 10% can be observed around 60° for the torsional angle ϕ of residue 5. Irrespective of the substituent at the β-C-atom, the ϕ dihedral-angle conformation around −120°, *i.e.* (−)-*ac*, is preferred over the conformation around 60°, *i.e.*, (+)-*sc*[1]).

Although the valine side chains seem not to have a significant effect on the structural preferences of the peptides investigated here, the question remains why the

[1]) The terms *ac* and *sc* denote *anticlinal* and *synclinal*, respectively.

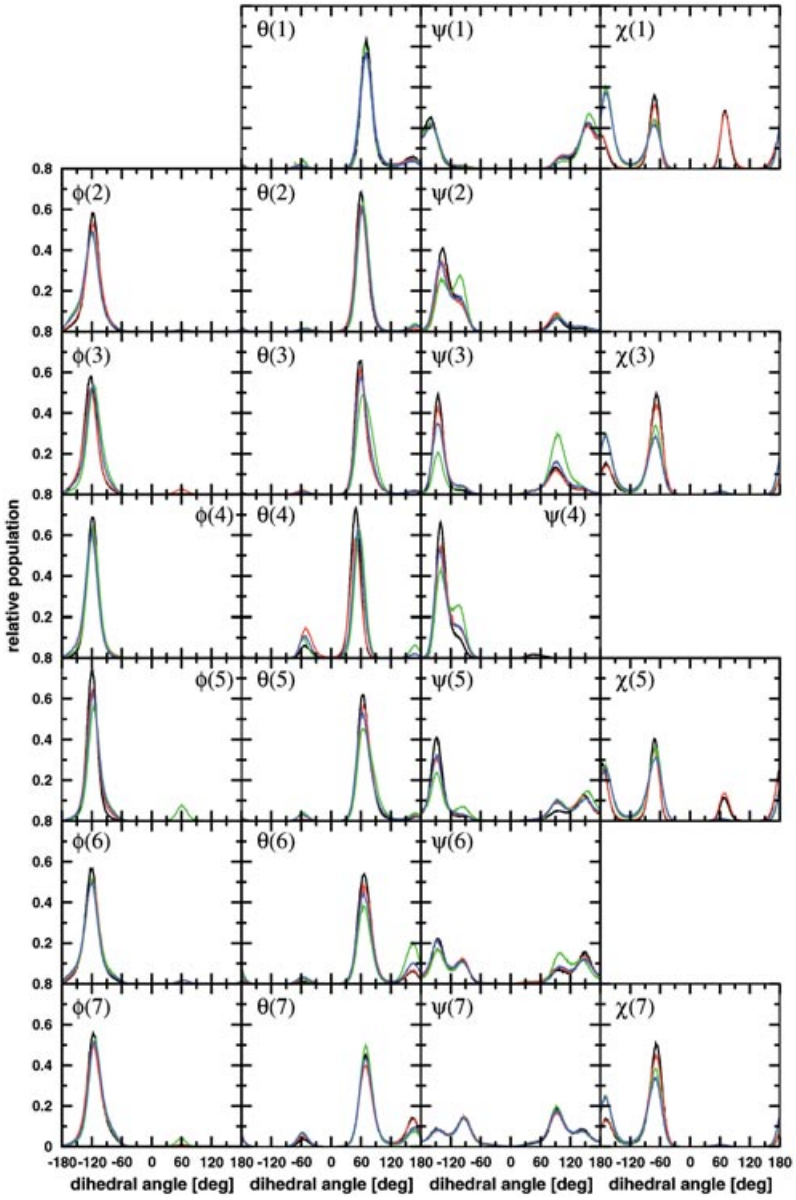

Fig. 8. *Normalized distribution of the values of the backbone and the first side-chain dihedral angles for residues 1–7 in the simulations of the peptides A_{val} and A_{leu} at 298 and 340 K*. Black, simulation $A_{val\text{-}298}$; red, simulation $A_{val\text{-}340}$; green, simulation $A_{leu\text{-}298}$; blue, simulation $A_{leu\text{-}340}$; ϕ, torsional dihedral angle C(O)–N–C_β–C_α; ϕ, torsional dihedral angle N–C_β–C_α–C(O); ψ, torsional dihedral angle C_β–C_α–C(O)–N; χ, torsional dihedral angle N–C_β–C_γ–C_δ.

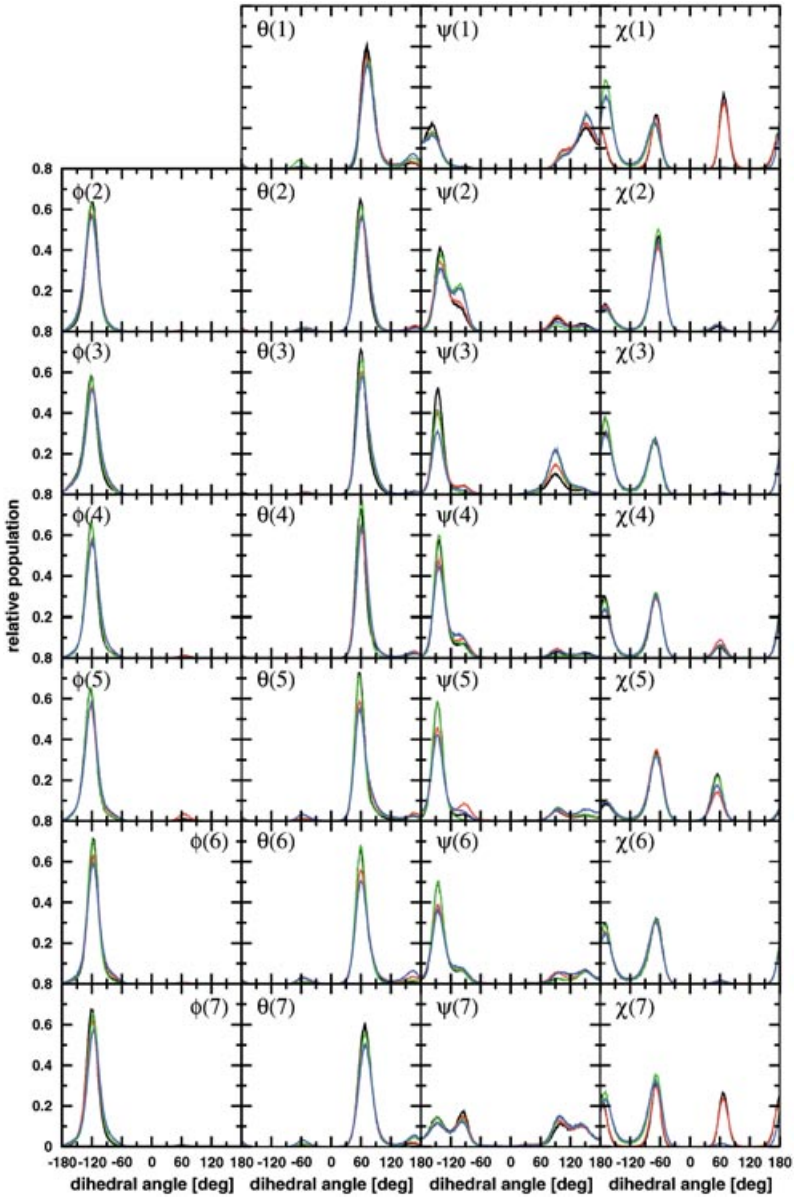

Fig. 9. *Normalized distribution of the values of the backbone and the first side-chain torsional angles for residues 1–7 in the simulations of the peptides B_{val} and B_{leu} at 298 and 340 K*. Black, simulation $B_{val\text{-}298}$; red, simulation $B_{val\text{-}340}$; green, simulation $B_{leu\text{-}298}$; blue, simulation $B_{leu\text{-}340}$. For the definition of the torsional dihedral angles ϕ, θ, ψ, and χ, see *Fig. 8.*

presence of valine side chains would result in a larger helical propensity in some cases. In *Fig. 10*, a systematic conformational analysis is shown for the valine side chain in β-amino acids, which represents a common approach to rationalize structural preferences

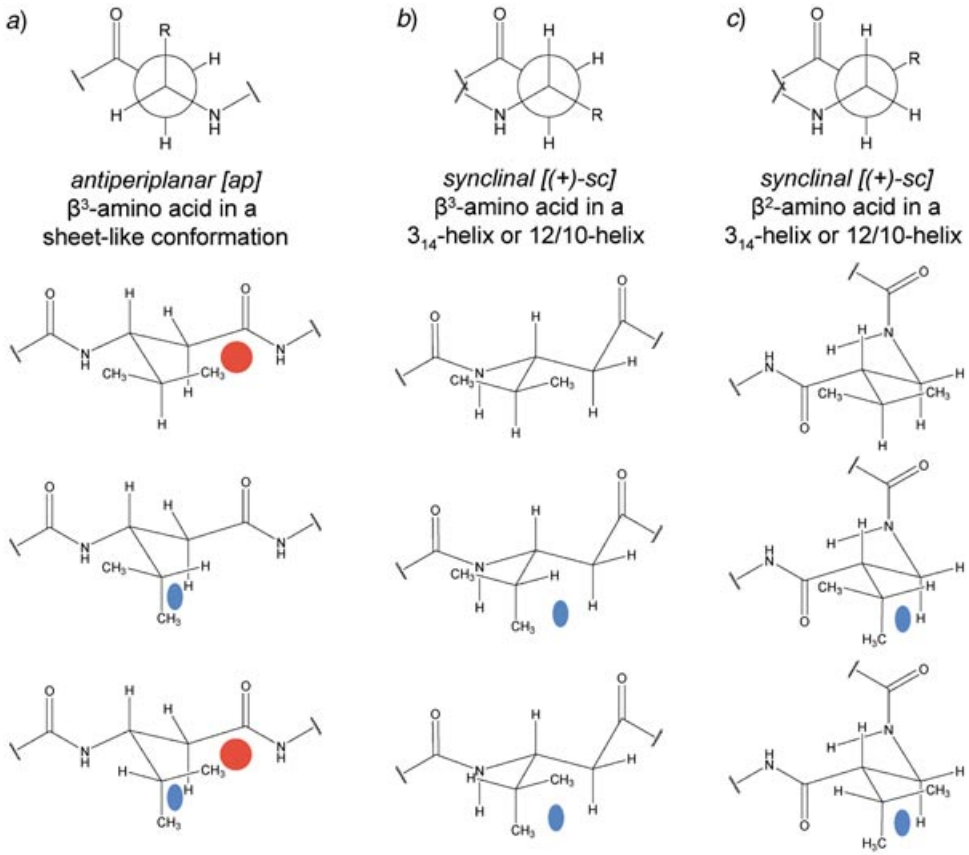

Fig. 10. *Systematic conformational analysis for the valine side chain in β-amino acids.* Panel *a* describes the situation for a β^3-valine residue in an extended backbone conformation, with the NH group in *antiperiplanar* (*ap*) conformation to the C=O group. Panel *b* describes the situation in a helical backbone conformation for a β^3-valine residue, with the NH group in a (+)-*synclinal* ((+)-*sc*) conformation. Panel *c* depicts the situation for a β^2-valine residue in a helical backbone conformation. In an extended backbone conformation, two out of three side-chain conformations are highly unfavorable due to massive 1,5-repulsions between a Me group and the C=O C-atom (red dots; 'forbidden' conformations); in the helical conformation, these 1,5-interactions do not occur. The blue dots denote 1,5-repulsions between Me groups and H-atoms, which are much less unfavorable. Thus, in a helical backbone conformation, valine side chains have more rotational freedom than in an extended conformation. This would ultimately lead to a preference for the helical conformation.

in organic chemistry [67]. The analysis suggests that the extended backbone (antiperiplanar) conformation of a residue with an α-branched side chain adjacent to the β-C-atom is destabilized relative to the helical (+)-*sc* conformation. However, this effect is certainly not the crucial factor for the 3_{14}-helical preference of β^3-peptides.

3. Conclusions. – We have investigated the effect of valine side chains on the folding/unfolding equilibrium of β^3-peptides and on their propensity for folding to a 3_{14}-helix by performing MD simulations on two different β^3-heptapeptides, A_{val} and B_{val}, and their 'valine-free' analogues A_{leu} and B_{leu}, respectively, at 298 and 340 K, starting

from fully extended conformations. In contrast to the conclusions drawn from a CD investigation [53], the presence or absence of valine side chains in β^3-peptides has no significant effect on the 3_{14}-helical propensity of the folding/unfolding behaviour in our simulations. All four peptides adopt a 3_{14}-helical conformation at both simulation temperatures. In all simulations, except for $A_{leu\text{-}298}$, the 3_{14}-helix represents the dominant conformation, and, in all simulations, it represents the conformation with the longest average lifetime. The folding behavior of the different peptides is rather similar and does not seem to be influenced by replacement of the valine by leucine side chains. No other well-defined secondary structure at a statistically relevant population is observed, and the populated conformational spaces of the peptides with and without valine side chains overlap to a very large degree. Although the 3_{14}-helix is generally less populated in the peptides without valine side chains, these differences are not necessarily due to the absence of side-chain branching adjacent to the β-C-atom. They may be mainly due to the possibility that, in a simulation of finite length, the relative conformer populations have not fully converged. Therefore, the estimated free energies of folding to the 3_{14}-helix have certainly not converged either, and should, thus, be interpreted with care.

It is certainly possible, as suggested by *Raguse et al.* [53], that conformations other than the 3_{14}-helix are accessible for β^3-peptides. However, these appear not to be dominant over the 3_{14}-helical conformations. Our results imply that the structural preference of β^3-peptides corresponds to the 3_{14}-helix independent of the presence of branched side chains adjacent to the β-C-atom. The observation made by *Martinek* and *Fülöp* [39] that i-Pr substituents on the β-C-atom restrict the torsional movement about the $N-C_\beta$ bond (the ϕ dihedral angle) and, thus, makes it more difficult to adopt gauche-(+) conformations, probably applies, but might be irrelevant to the structural preference of β^3-peptides. In a similar vein, the destabilization of the extended backbone conformation in the presence of valine side chains seems, in general, not to be decisive for the formation of a 3_{14}-helical conformation. The conformational preference of the ϕ torsion is found in the MD simulations to be *ca.* $-120°$ for all residues, while the θ torsion predominantly results in a (+)-*sc* conformation irrespective of the type of substituent. Dihedral-angle conformations of the torsion ϕ near $60°$ are only poorly populated.

It goes without saying that the results presented here highly depend on the force field used, and one might think that the GROMOS force field favors the formation of 3_{14}-helices of β-peptides over other folded conformations. However, we wish to emphasize that GROMOS is parametrized against thermodynamic properties such as density and heat of vaporization of liquids of small organic molecules, and against crystallographic data of natural α-amino acids, and *not* against the structural preferences of α- or β-peptides. Furthermore, GROMOS has, in agreement with experimental findings, very well reproduced the structural preference of various peptides [10][17][46][47][50][58][63][68–70], and not only of β-peptides adopting a 3_{14}-helix.

Experimental Part

Molecular Model. The β-peptides were modeled with the GROMOS96 biomolecular force field, parameter set 45A3 [64][65] along the lines described by *Daura et al.* [13]. Aliphatic CH_n groups were treated as united atoms, both in the peptides and the solvent. Both the N- and the carboxylic acid C-termini were protonated, in

line with experimental data. MeOH was modeled by means of the standard GROMOS96 set of solvents [64] as a rigid three-site model, whose properties agree well with experiment [71].

Simulation Setup. All MD simulations presented here were carried out with the GROMOS96 suite of programs [64][66]. For all peptides, the initial structure was fully extended (all backbone dihedral angles set to 180°) and solvated in a truncated-octahedron-shaped box, assuring an initial minimum distance of 1.4 nm between the peptide and the square walls of the truncated octahedron. Periodic boundary conditions were applied.

After relaxation of the systems using steepest-descent energy minimization, the MD simulations were started by taking the initial velocities from a *Maxwellian* distribution at 298 K. Solvent and solute were independently coupled to a temperature bath with a relaxation time of 0.1 ps [72]. The pressure was calculated with a molecular virial, and held constant at an isothermal compressibility of $4.575 \cdot 10^{-4}$ (kJ mol^{-1} nm^{-3})$^{-1}$. Bond lengths were constrained with the SHAKE algorithm [73], allowing a geometric tolerance of 10^{-4}. The equations of motion were integrated using the leap-frog algorithm and a time step of 2 fs. The interaction between atoms in so-called charge groups [64] was calculated according to a spherical triple-range cutoff scheme: short-range *Van der Waals* and electrostatic interactions were evaluated at every time step by means of a charge-group pair list generated with a short-range cutoff radius of 0.8 nm between the centers of geometry of the peptide charge groups and the O-atoms of the solvent molecules (MeOH). Longer-range *Van der Waals* and electrostatic interactions, between pairs at a distance longer than 0.8 nm and shorter than a long-range cutoff of 1.4 nm, were evaluated every fifth time step, at which point the pair list was also updated, and were kept unchanged between these updates. To approximate the electrostatic interactions beyond the long-range cutoff, a *Poisson–Boltzmann* reaction-field force was used. The value for the dielectric permittivity of the continuum outside the long-range cutoff was set to 17.7, corresponding to the value for the dielectric permittivity of the MeOH model [71] used. The simulations were equilibrated for 1 ns, and the following 100 to 200 ns were used for analysis, saving configurations every 0.5 ps.

Analysis. Least-squares translational and rotational fitting of atomic coordinates for the calculation of the root-mean-square-differences (rmsd) was based on the backbone atoms (N, C_β, C_α, C) of residues 2 to 6. A conformational-clustering analysis was performed as described by *Daura et al.* [58] on the set of all peptide structures taken at 0.01-ns intervals from the simulation. The backbone atom-positional rmsd was used as a similarity criterion. A maximum cluster radius of 0.1 nm was chosen, corresponding to the cluster radius commonly used for β-heptapeptides [58]. To identify the set of structures from the simulation that would be representative for the 3_{14}-helical conformation, either a canonical 3_{14}-helix or the NMR model structure, where available, was imposed during the clustering procedure as central member of a cluster, referred to as 'cluster 0'. This arbitrary choice of the central member structure of one of the clusters prevents the 3_{14}-helical conformations to be distributed over more than one cluster.

Folding free energies were calculated as:

$$\Delta G_{\text{folding}} = k_B T \ln \frac{P_{\text{folded}}}{P_{\text{unfolded}}}$$

where k_B is the *Boltzmann* constant, T is the temperature, and P_{folded} and P_{unfolded} are the relative probabilities of finding the system in the folded and unfolded conformations, respectively. P_{folded} and P_{unfolded} can be approximated by the relative number of folded and unfolded structures, respectively, in the simulation. The folded structures refer to the members of a cluster (the 3_{14}-helical cluster or the most-populated cluster), whereas the unfolded structures then refer to the group of the remaining clusters. The average lifetime of a conformer was calculated by recording the times at which the conformer was accessed and left again. When a conformer was left and accessed within 20 ps, the sampling of the conformer was considered to be continuous. The average time of (re)folding to the 3_{14}-helix, and the average number of conformers visited during a (re)folding process, are calculated from a subset of folding events involving more than one intermediate conformer. H-bonds were calculated based on a geometric criterion: a H-bond was defined by a minimum donor–H-atom–acceptor angle of 135°, and a maximum H-atom–acceptor distance of 0.25 nm.

Financial support by the *National Center of Competence in Research* (*NCCR*) *Structural Biology* of the *Swiss National Science Foundation* (*SNSF*) is gratefully acknowledged.

REFERENCES

[1] S. H. Gellman, *Acc. Chem. Res.* **1998**, *31*, 173.
[2] D. J. Hill, M. J. Mio, R. B. Prince, T. S. Hughes, J. S. Moore, *Chem. Rev.* **2001**, *101*, 3893.
[3] D. Seebach, J. L. Matthews, *Chem. Commun.* **1997**, *79*, 2015.
[4] K. Gademann, T. Hintermann, J. V. Schreiber, *Curr. Med. Chem.* **1999**, *6*, 905.
[5] R. P. Cheng, S. H. Gellman, W. F. DeGrado, *Chem. Rev.* **2001**, *101*, 3219.
[6] S. Krauthäuser, L. A. Christianson, D. R. Powell, S. H. Gellman, *J. Am. Chem. Soc.* **1997**, *119*, 11719.
[7] D. Seebach, S. Abele, T. Sifferlen, M. Hänggi, S. Gruner, P. Seiler, *Helv. Chim. Acta* **1998**, *81*, 2218.
[8] D. Seebach, S. Abele, K. Gademann, B. Jaun, *Angew. Chem., Int. Ed.* **1999**, *38*, 1595.
[9] Y. J. Chung, B. R. Huck, L. A. Christianson, H. E. Stanger, S. Krauthäuser, D. R. Powell, S. H. Gellman, *J. Am. Chem. Soc.* **2000**, *17*, 3995.
[10] X. Daura, K. Gademann, H. Schäfer, B. Jaun, D. Seebach, W. F. van Gunsteren, *J. Am. Chem. Soc.* **2001**, *123*, 2393.
[11] D. Seebach, M. Overhand, F. N. M. Kühnle, B. Martinoni, L. Oberer, U. Hommel, H. Widmer, *Helv. Chim. Acta* **1996**, *79*, 913.
[12] D. Seebach, P. E. Ciceri, M. Overhand, B. Jaun, D. Rigo, L. Oberer, U. Hommel, H. Widmer, *Helv. Chim. Acta* **1996**, *79*, 2043.
[13] X. Daura, W. F. van Gunsteren, D. Rigo, B. Jaun, D. Seebach, *Chem.–Eur. J.* **1997**, *3*, 1410.
[14] P. I. Arvidsson, M. Rueping, D. Seebach, *Chem. Commun.* **2001**, *7*, 649.
[15] T. Etezady-Esfarjani, C. Hilty, K. Wüthrich, M. Rueping, J. V. Schreiber, D. Seebach, *Helv. Chim. Acta* **2002**, *85*, 1197.
[16] D. Seebach, S. Abele, K. Gademann, G. Guichard, T. Hintermann, B. Jaun, J. L. Matthews, J. V. Schreiber, L. Oberer, U. Hommel, H. Widmer, *Helv. Chim. Acta* **1998**, *81*, 932.
[17] X. Daura, K. Gademann, B. Jaun, D. Seebach, W. F. van Gunsteren, A. E. Mark, *Angew. Chem., Int. Ed.* **1999**, *38*, 236.
[18] M. Rueping, J. V. Schreiber, G. Lelais, B. Jaun, D. Seebach, *Helv. Chim. Acta* **2002**, *85*, 2577.
[19] T. D. W. Claridge, J. M. Goodman, A. Moreno, D. Angus, S. F. Barker, C. Taillefumier, M. P. Watterson, G. W. J. Fleet, *Tetrahedron Lett.* **2001**, *42*, 4251.
[20] D. H. Appella, L. A. Christianson, I. L. Karle, D. R. Powell, S. H. Gellman, *J. Am. Chem. Soc.* **1996**, *118*, 13071.
[21] D. H. Appella, L. A. Christianson, D. A. Klein, D. R. Powell, X. Huang, J. J. Brachi Jr., S. H. Gellman, *Nature (London)* **1997**, *387*, 381.
[22] D. Seebach, S. Abele, J. V. Schreiber, B. Martinoni, A. K. Nussbaum, H. Schild, H. Schulz, H. Hennecke, R. Woessner, F. Bitsch, *Chimia* **1998**, *52*, 734.
[23] D. Seebach, M. Albert, P. I. Arvidsson, M. Rueping, J. V. Schreiber, *Chimia* **2001**, *55*, 345.
[24] J. Frackenpohl, P. I. Arvidsson, J. V. Schreiber, D. Seebach, *ChemBioChem* **2001**, *2*, 445.
[25] D. F. Hook, F. Gessier, C. Noti, P. Kast, D. Seebach, *ChemBioChem* **2004**, *5*, 691.
[26] N. Umezawa, M. A. Gelman, M. C. Haigis, R. T. Raines, S. H. Gellman, *J. Am. Chem. Soc.* **2002**, *124*, 368.
[27] M. Rueping, Y. Majahan, M. Sauer, D. Seebach, *ChemBioChem* **2002**, *3*, 257.
[28] D. Seebach, K. Namoto, Y. Mahajan, P. Bindschädler, R. Sustmann, M. Kirsch, N. S. Ryder, M. Weiss, M. Sauer, C. Roth, S. Werner, H.-D. Beer, C. Munding, P. Walde, M. Voser, *Chem. Biodiv.* **2004**, *1*, 65.
[29] Y. Hamuro, J. P. Schneider, W. F. DeGrado, *J. Am. Chem. Soc.* **1999**, *121*, 12200.
[30] E. A. Porter, X. Wang, H.-S. Lee, B. Weisblum, S. H. Gellman, *Nature (London)* **2000**, *404*, 565.
[31] D. Liu, W. F. DeGrado, *J. Am. Chem. Soc.* **2001**, *123*, 7553.
[32] P. I. Arvidsson, J. Frackenpohl, N. S. Ryder, B. Liechty, F. Petersen, H. Zimmermann, G. P. Camenisch, R. Woessner, D. Seebach, *ChemBioChem* **2001**, *10*, 771.
[33] P. I. Arvidsson, N. S. Ryder, H. M. Weiss, G. Gross, O. Kretz, R. Woessner, D. Seebach, *ChemBioChem* **2003**, *4*, 1345.
[34] M. Werder, H. Hauser, S. Abele, D. Seebach, *Helv. Chim. Acta* **1999**, *82*, 1774.
[35] K. Gademann, M. Ernst, D. Hoyer, D. Seebach, *Angew. Chem., Int. Ed.* **1999**, *38*, 1223.
[36] K. Gademann, M. Ernst, D. Seebach, D. Hoyer, *Helv. Chim. Acta* **2000**, *83*, 16.
[37] K. Gademann, T. Kimmerlin, D. Hoyer, D. Seebach, *J. Med. Chem.* **2001**, *44*, 2460.
[38] C. Nunn, M. Rueping, D. Langenegger, E. Schuepbach, E. Kimmerlin, P. Micuch, K. Hurth, D. Seebach, D. Hoyer, *Arch. Pharmacol.* **2003**, *367*, 95.
[39] T. A. Martinek, F. Fülöp, *Eur. J. Biochem.* **2003**, *270*, 3657.

[40] K. Möhle, R. Günther, M. Thormann, N. Sewald, H.-J. Hofmann, *Biopolymers* **1999**, *50*, 167.
[41] R. Günther, H.-J. Hofmann, *Helv. Chim. Acta* **2002**, *85*, 2149.
[42] Y.-D. Wu, D.-P. Wang, *J. Am. Chem. Soc.* **1998**, *120*, 13485.
[43] Y.-D. Wu, D.-P. Wang, *J. Am. Chem. Soc.* **1999**, *121*, 9352.
[44] Y.-D. Wu, J.-Q. Lin, Y.-L. Zhao, *Helv. Chim. Acta* **2002**, *85*, 3144.
[45] W. F. DeGrado, J. P. Schneider, Y. Hamuro, *J. Pept. Res.* **1999**, *54*, 206.
[46] X. Daura, B. Jaun, D. Seebach, W. F. van Gunsteren, A. Mark, *J. Mol. Biol*. **1998**, *280*, 925.
[47] C. Peter, M. Rueping, H. J. Wörner, B. Jaun, D. Seebach, W. F. van Gunsteren, *Chem.–Eur. J.* **2003**, *9*, 5838.
[48] D. Seebach, T. Sifferlen, P. A. Mathieu, A. M. Häne, C. M. Krell, D. J. Bierbaum, S. Abele, *Helv. Chim. Acta* **2000**, *83*, 2849.
[49] D. Seebach, T. Sifferlen, D. J. Bierbaum, M. Rueping, B. Jaun, B. Schweizer, J. Schaefer, A. K. Mehta, R. D. O'Connor, B. H. Meier, M. Ernst, A. Glättli, *Helv. Chim. Acta* **2002**, *85*, 2877.
[50] A. Glättli, X. Daura, D. Seebach, W. F. van Gunsteren, *J. Am. Chem. Soc.* **2002**, *124*, 12972.
[51] D. Seebach, K. Gademann, J. V. Schreiber, J. L. Matthews, T. Hintermann, B. Jaun, L. Oberer, U. Hommel, H. Widmer, *Helv. Chim. Acta* **1997**, *80*, 2033.
[52] M. Rueping, Y. Majahan, B. Jaun, D. Seebach, *Chem.–Eur. J.* **2004**, *10*, 1607.
[53] T. L. Raguse, J. R. Lai, S. H. Gellman, *Helv. Chim. Acta* **2002**, *85*, 4154.
[54] B. W. Gung, D. Zou, A. M. Stalcup, C. E. Cottrell, *J. Org. Chem*. **1999**, *64*, 2176.
[55] D. Seebach, J. V. Schreiber, S. Abele, X. Daura, W. F. van Gunsteren, *Helv. Chim. Acta* **2000**, *83*, 34.
[56] J. V. Schreiber, D. Seebach, *Helv. Chim. Acta* **2000**, *83*, 3139.
[57] D. Seebach, J. V. Schreiber, P. I. Arvidsson, J. Frackenpohl, *Helv. Chim. Acta* **2001**, *84*, 271.
[58] X. Daura, W. F. van Gunsteren, A. E. Mark, *Proteins: Struct., Funct., Genet.* **1999**, *34*, 269.
[59] W. F. van Gunsteren, R. Bürgi, C. Peter, X. Daura, *Angew. Chem., Int. Ed*. **2001**, *40*, 351.
[60] X. Daura, A. Glättli, P. Gee, C. Peter, W. F. van Gunsteren, *Adv. Protein Chem.* **2002**, *62*, 341.
[61] X. Daura, I. Antes, W. F. van Gunsteren, A. E. Mark, *Proteins: Struct., Funct., Genet*. **1999**, *36*, 542.
[62] X. Daura, A. E. Mark, W. F. van Gunsteren, *Comput. Phys. Commun*. **1999**, *123*, 97.
[63] C. Peter, X. Daura, W. F. van Gunsteren, *J. Biomol. NMR* **2001**, *20*, 297.
[64] W. F. van Gunsteren, S. R. Billeter, A. A. Eising, P. H. Hünenberger, P. Krüger, A. E. Mark, W. R. P. Scott, I. G. Tironi, 'Biomolecular Simulation: The GROMOS96 Manual and User Guide', vdf Hochschulverlag, ETH Zürich, Switzerland, 1996.
[65] L. Schuler, X. Daura, W. F. van Gunsteren, *J. Comput. Chem*. **2001**, *22*, 1205.
[66] W. R. P. Scott, P. H. Hünenberger, I. G. Tironi, A. E. Mark, S. R. Billeter, J. Fennen, A. Torda, T. Huber, P. Krüger, W. F. van Gunsteren, *J. Phys. Chem*. **1999**, *103*, 3596.
[67] G. Quinkert, E. Egert, C. Griesinger, 'Aspects of Organic Chemistry – Structure', Verlag Helvetica Chimica Acta, Basel, Switzerland, 1996.
[68] C. Peter, X. Daura, W. F. van Gunsteren, *J. Am. Chem. Soc*. **2000**, *122*, 7461.
[69] R. Bürgi, X. Daura, A. E. Mark, M. Bellanda, B. Mammi, E. Peggion, W. F. van Gunsteren, *J. Pept. Res.* **2001**, *57*, 107.
[70] H. Yu, X. Daura, W. F. van Gunsteren, *Proteins: Struct., Funct., Bioinf.* **2004**, *54*, 116.
[71] R. Walser, A. E. Mark, W. F. van Gunsteren, M. Lauterbach, G. Wipff, *J. Chem. Phys.* **2000**, *112*, 10450.
[72] H. J. C. Berendsen, J. P. M. Postma, W. F. van Gunsteren, A. DiNola, J. R. Haak, *J. Chem. Phys.* **1984**, *81*, 3684.
[73] J.-P. Ryckaert, G. Ciccotti, H. J. C. Berendsen, *J. Comput. Phys.* **1977**, *23*, 327.

Received June 18, 2004